SUPPLEMENTARY DATA

Probing the role of ligation and exonuclease digestion towards non-specific amplification in bioanalytical RCA assays

Vandana Kuttappan Nair*[ab#], Chandrika Sharma[ab#], Shrawan Kumar[ab], Mrittika Sengupta[a], Souradyuti Ghosh**[ab]

[a], Centre for Life Sciences, Mahindra University, Hyderabad, Telangana, India

[b], Interdisciplinary Centre for Nanosensors and NanoMedicine, Mahindra University, Hyderabad, Telangana, India

*, Corresponding author

**, Corresponding author, will handle communications (souradyutighoshacademic@gmail.com, souradyuti.ghosh@mahindrauniversity.edu.in)

[#], joint 1st authors.

Table of Content

Abbreviations: Circular DNA: cDNA; NSA: non-specific amplification; NNSA: normalized non-specific amplification; Exo I: Exonuclease I; Exo III: Exonuclease III; RFU: relative fluorescence units.

Supporting Information Section – 1: Various ligation techniques for making pre-synthesized circular DNA (cDNA) and their bioanalytical RCA applications

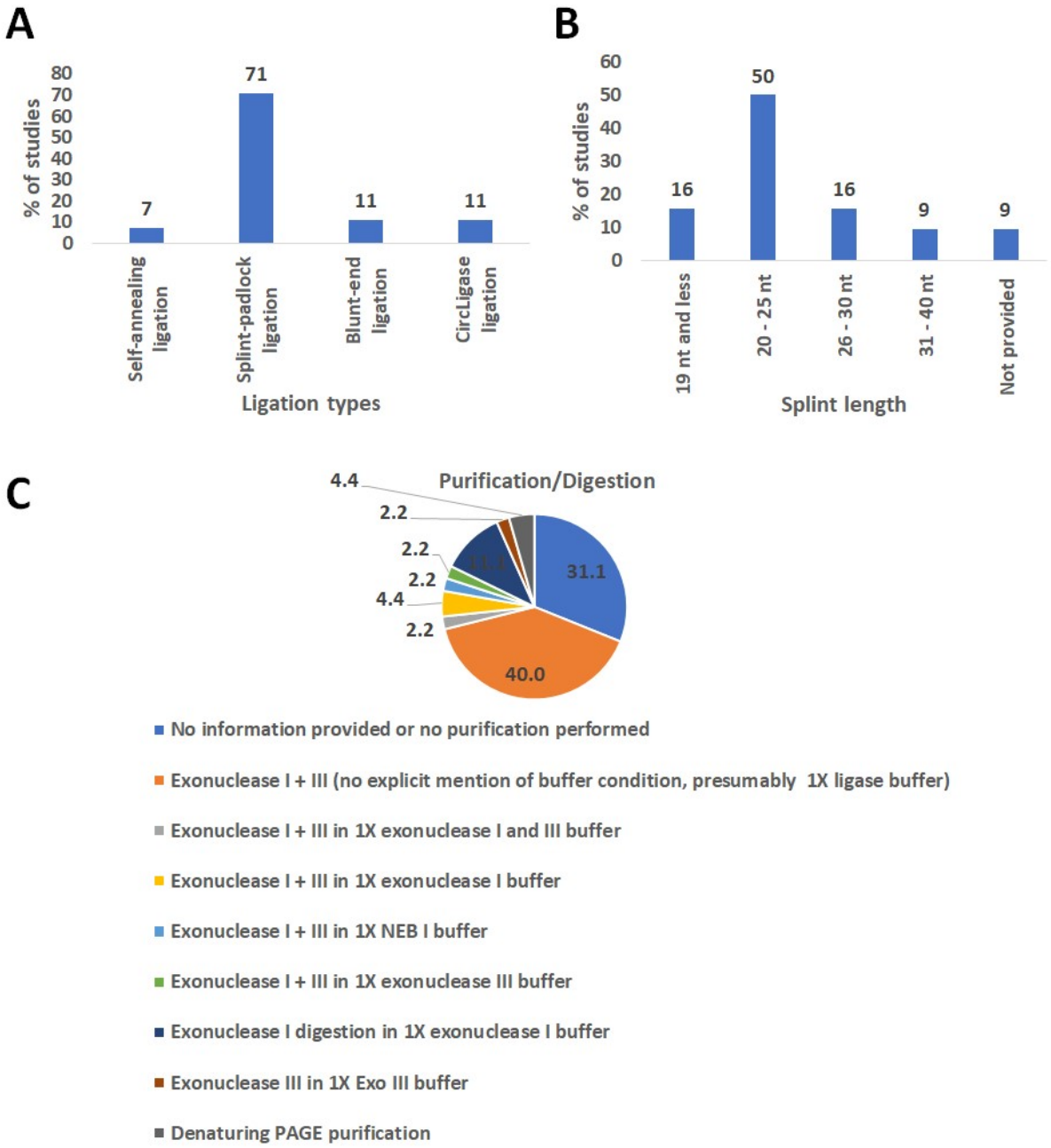

Figure S1. Survey of existing reports from NCBI Pubmed (from January 2017 to May 2021) for preparing pre-synthesized circular DNA for an RCA-based bioanalytical study. The search keywords used were "Rolling AND circle AND amplification". Only the publications using presynthesized circular DNA are used for this survey. A, Representation of studies using different ligation techniques. B, Representation of studies using different splint lengths employed for splint-padlock ligation. C, Representation (in terms of % of papers) of studies using different digestion and purification techniques utilized for the removal of unligated precursor oligonucleotides. The papers used in preparing these charts are listed under references[1–46].

1.1 Bioanalytical RCA applications of cDNAs from various ligations. In self-annealing ligation, the 5′- and 3′-termini of a 5′-phosphorylated oligonucleotide are brought in proximity by intramolecular

annealing. A DNA ligase joining the termini leads to self-annealing ligation, forming cDNA with applications such as detecting leukaemia biomarker BCR/ABLp210 fusion[47] (Scheme 1A). In the splint-padlock ligation, an oligonucleotide "splint" (could be a DNA or RNA) anneals to another 5′-phosphorylated oligonucleotide "padlock" to bring 5′- and 3′-terminus of the latter to immediate proximity (Scheme 1B). A DNA or RNA ligase (depending on the splint) then joins the termini, creating a cDNA. Splint-padlock ligation remains the most attractive method for circular DNA (cDNA) preparation, including a recent work involving thrombin detection[23]. Another method of preparing cDNA involves cohesive end ligation (Scheme 1C), where the 5′- and 3′-termini are brought in proximity for ligation using complementary overhangs called "cohesive ends" or "sticky-ends"[48]. Such cohesive ends can be generated by enzymatic digestion or deliberate sequence design, followed by ligation to enable circularization[49]. RCA assays involving cohesive end ligated cDNAs have been applied to detect thrombin and let-7 family miRNA[48,49].

Supporting Information Section – 2: Oligonucleotide sequences and secondary structures

Table S1. List, sequences, and description of oligonucleotides used in this study

Oligonucleotide	Sequence (5′ to 3′)	Description
1	GTC GCT TTT AGA GTA GAT GAG TGC AAG CCT TTA GCG ACG TCC AGT CCA TCC AGT CGT CGA TCG TTC CTA AGT CCA CTA CAC CAT GCG TAC CTC AGC TTT GGA CTG GAC	Precursor to self-annealing ligated circular DNA (cDNA) **1C**
2	TAC GCA TGG TGT AGT GGA CT	Primer sequence for cDNA **1C**. Please note that this oligonucleotide is also the primer for cohesive end ligated circular DNAs **11C** – **13C**
3	CCA GTC GTC GAT CGT	HRCA primer sequence for cDNA **1C**
4	GTGCCGGAGTACCTGACCTGCAGTGACG GT GACAGACAAACGAGCTATACTTCGCAGT GAC GGTCGAGTTCGCGGTCGGTCTGACGCAG TGA CGCCGTAAGATGCACCTCAT	Padlock precursor to splint-padlock ligated cDNA **4C**
5	AGG TCA GGT ACT CCG GCA CAT GAG GTG CAT CTT ACG GC	38 nt splint for padlock precursor **4**
6	CAG GTA CTC CGG CAC ATG AGG TGC ATC TTA	30 nt splint for padlock precursor **4**
7	GTA CTC CGG CAC ATG AGG TGC ATC	24 nt splint for padlock precursor **4**
8	TCC GGC ACA TGA GGT G	16 nt splint for padlock precursor **4**
9	CAG ACC GAC CGC GAA CTC GAC C	Primer sequence for cDNA **4C**
10	GGT GAC AGA CAA ACG AGC TAT ACT TC	HRCA primer sequence for cDNA **4C**
11a	CTG CAT CTC CAC TGC TGA ATT CTT TTG AGT AGT TTG AAT TCA G	First precursor to cohesive end ligated cDNA **11C** (14 nt cohesive end at 5′-side)
11b	CAG TGG AGA TGC AGC TGG ATC CTC CCT CCC TCC CTC CCA GTA AGT CCA CTA CAC CAT GCG TAT TTG GAG GAT CCA G	Second precursor to cohesive end ligated cDNA **11C** (14 nt cohesive end at 5′-side)
12a	CAT CCA CTC CTG AAT TCT TTT GAG TAG TTT GAA TTC AG	First precursor to cohesive end ligated cDNA **12C** (9 nt cohesive end at 5′-side)
12b	GAG TGG ATG CTG GAT CCT CCC TCC CTC CCT CCC AGT AAG TCC ACT ACA CCA TGC GTA TTT GGA GGA TCC AG	Second precursor to cohesive end ligated cDNA **12C** (9 nt cohesive end at 5′-side)
13a	CCA TCC TGA ATT CTT TTG AGT AGT TTG AAT TCA G	First precursor to cohesive end ligated cDNA **13C** (5 nt cohesive end at 5′-side)
13b	GAT GGC TGG ATC CTC CCT CCC TCC CTC CCA GTA AGT CCA CTA CAC CAT GCG TAT TTG GAG GAT CCA G	Second precursor to cohesive end ligated cDNA **13C** (5 nt cohesive end at 5′-side)
14	CCT CCC TCC CTC CCA	HRCA primer sequence for cDNAs **11C** – **13C**
15	CAC TGG ACG AGC TGA GGT GGG AGT AGG GAA GCT GAG GAA GGT CGA GTT CGC GGT CGG TCT GAC AAA TGA GGG GCT GAG GCA CGT CCA GTG GCG TGC TCA AAA AAA AAA AGA GCA CGC	Precursor for self-annealing ligated DNA **15C**

16	TCG TCG ACG GAT CCA TGG CAC ATG GAT TAC TAG CGA ACG CAT GAG CCG GCT GCG GCG CAT GCG T	Padlock precursor for splint-padlock ligated DNA **16C**
17	GC CAT GGA TCC GTC GAC GAA CGC ATG CGC CGC AGC CGG	38 nt splint for splint-padlock ligated DNA **16C**
18	CGT CGA CGA ACG CAT GCG	18 nt splint for splint-padlock ligated DNA **16C**
19	CTC AGC TTC CCT ACT CCC ACC	Primer for cDNA **15C**
20	GTT CGC TAG TAA TCC ATG	Primer for cDNA **16C**

2.1 Secondary structure generation conditions. In UNAFold[50], the secondary structures were generated by incorporating the oligonucleotide sequences in the "DNA Folding Form", with "sequence type" as circular, "Ionic Conditions" of 0.05 M NaCl, and 37°C "Temperature" option.

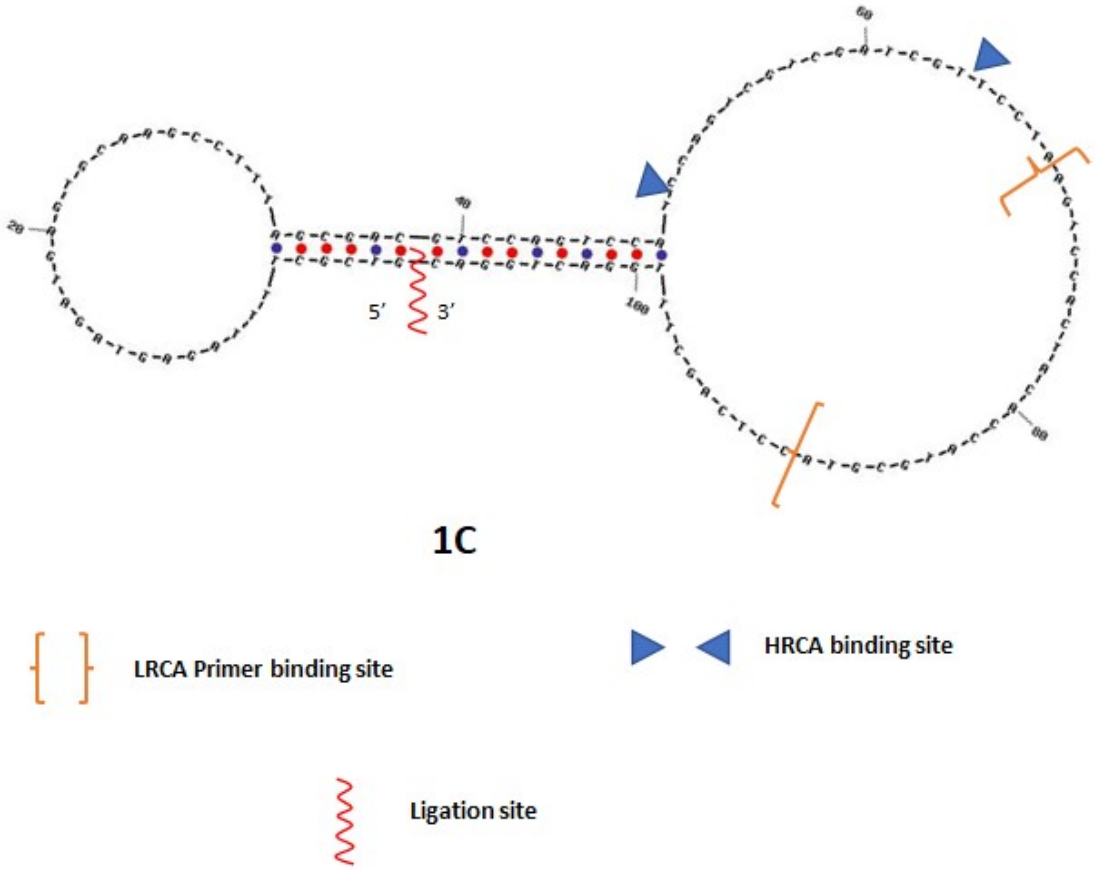

Figure S2. Secondary structure of self-annealing cDNA **1C**. The positions of the ligation site, primer, and HRCA primer binding sites are indicated. Secondary structure has been generated using UNAFold with 37°C temperature and 50 mM Na^+ salt condition[54].

2.2 Sequence design consideration for self-annealing cDNA. To prepare a dumbbell-shaped cDNA **1C** with self-annealed ligation, the stem regions of the precursor oligonucleotide **1** must fold into a stable duplex to bring 5′-PO_4 and 3′-OH termini in proximity (Scheme 1A). Furthermore, the loop region sequences were chosen to be predominantly free of any secondary structure. The presence of secondary structures in the loop region of **1C** and folding stability of the stem region as duplex were checked using UNAFold (IDT) simulation (Figure S2)[50,51]. The binding regions for LRCA and HRCA primers have been indicated.

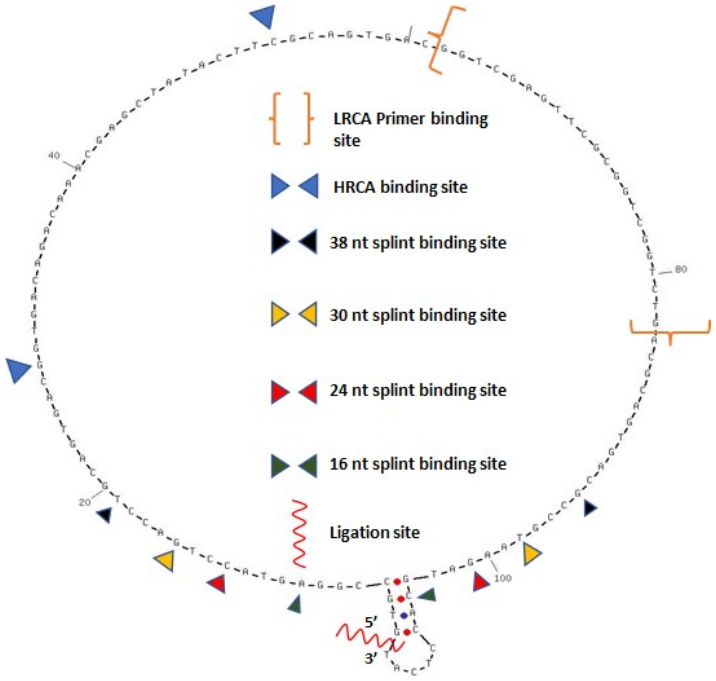

Figure S3. Secondary structure of splint-padlock ligated cDNA **4C**. The positions of the ligation site, splint-binding sites, primer, and HRCA primer binding sites are indicated. Secondary structure has been generated using UNAFold with 37°C temperature and 50 mM Na^+ salt condition[54].

2.3 Design consideration for padlock sequence and role of splint length. Initially, a 38 nt long splint was utilized to produce cDNA **4C**. Additionally, the role of splint length was investigated using shorter splints (30, 24, and 16 nt, oligonucleotides **6** – **8**, respectively) without changing the final cDNA sequence **4C** itself or the ligation site (Figure S3). The binding regions for LRCA and HRCA primers have been indicated.

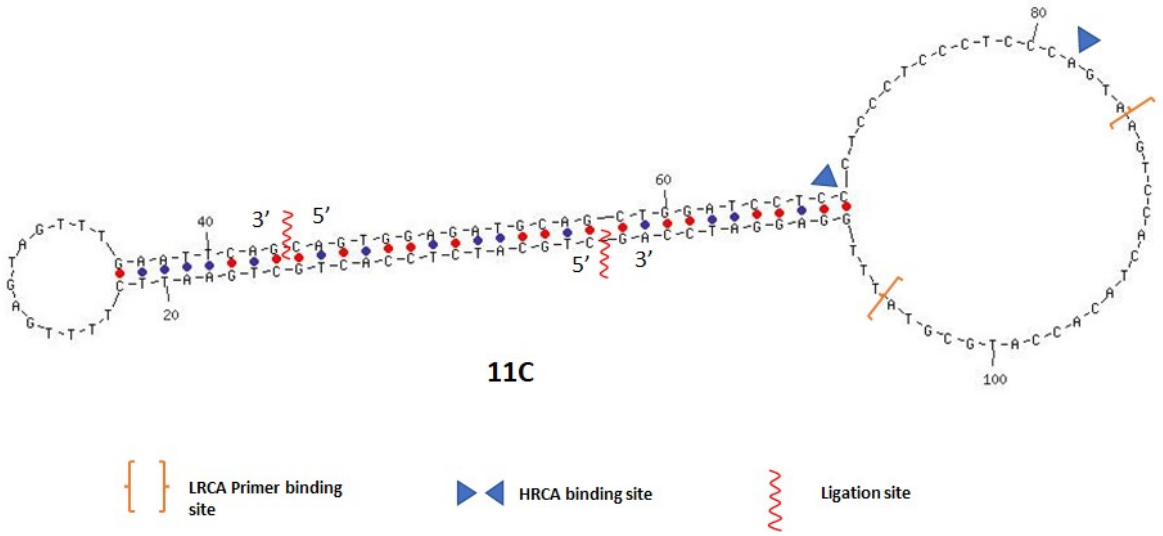

Figure S4. Secondary structure of cohesive end (14 nt cohesive end) cDNA **11C**. The positions of ligation site, primer and HRCA primer binding sites are indicated. Secondary structure has been generated using UNAFold with 37°C temperature and 50 mM Na^+ salt condition[54].

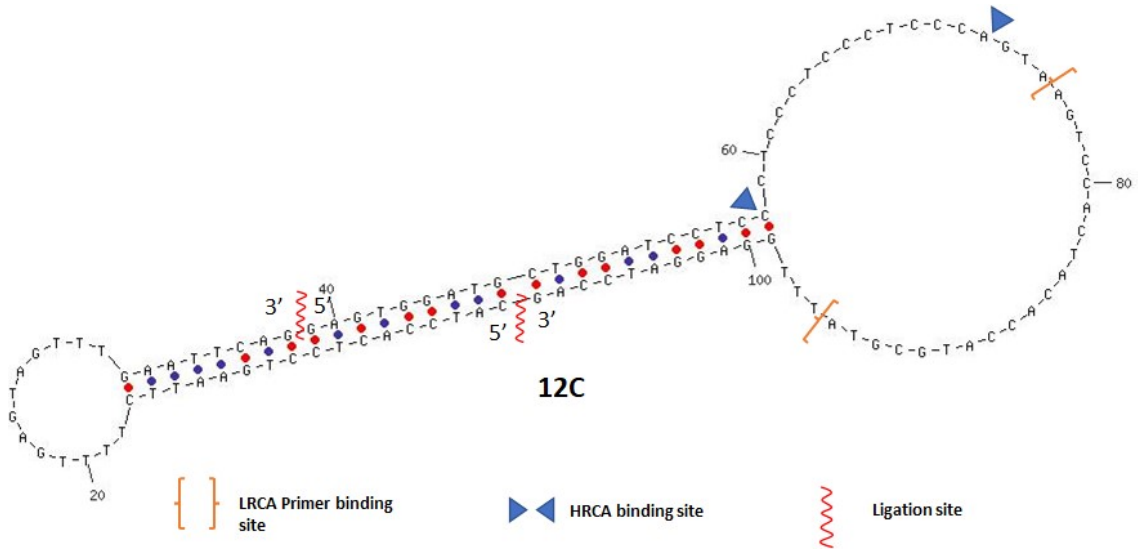

Figure S5. Secondary structure of cohesive end (9 nt cohesive end) circular DNA **12C**. The positions of the ligation site, primer, and HRCA primer binding sites are indicated. Secondary structure has been generated using UNAFold with 37°C temperature and 50 mM Na^+ salt condition[54].

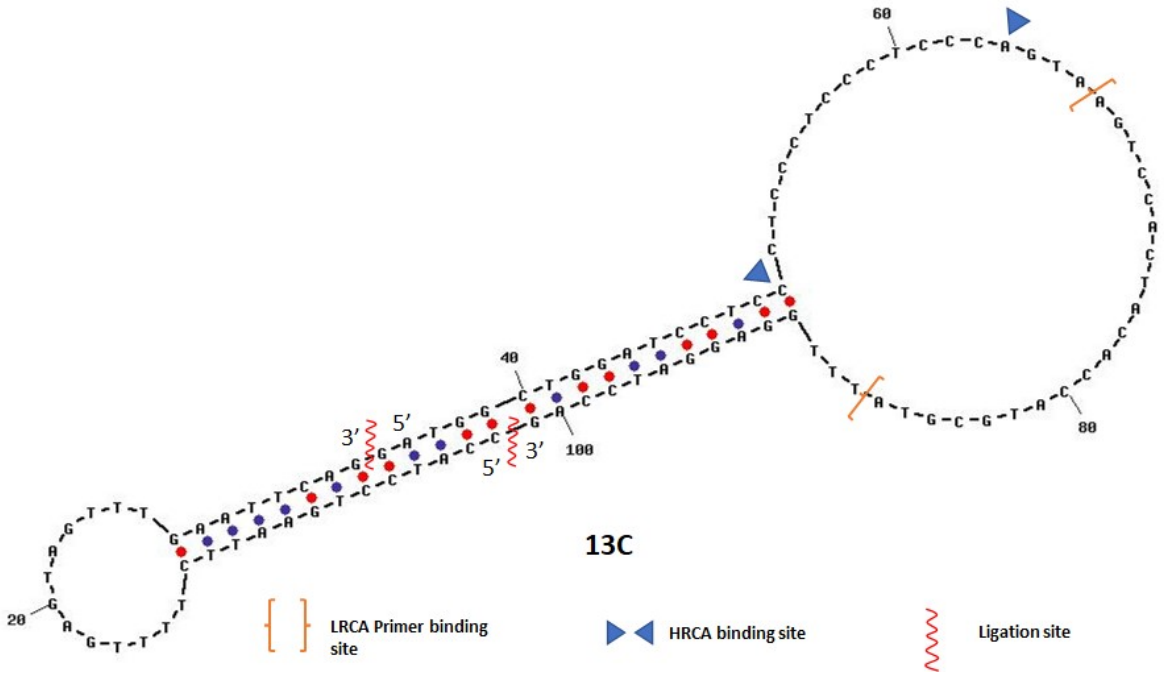

Figure S6. Secondary structure of cohesive end (5 nt cohesive end) cDNA **13C**. The positions of the ligation site, primer, and HRCA primer binding sites are indicated. Secondary structure has been generated using UNAFold with 37°C temperature and 50 mM Na^+ salt condition[54].

2.4 Sequence design consideration for cohesive end ligation. A set of non-palindromic cohesive end sequences was utilized for the cohesive end ligation. This way, two asymmetric precursor ssDNA fragments (**11a**/**11b**) containing these cohesive ends at 5′-termini would anneal into a stable asymmetric dumbbell-shaped duplex **11C** (Scheme 1C and Figure S4). For investigating the role of cohesive end overhang length in NSA, we also utilized precursors having 9 and 5 nt 5′-overhangs (**12a**/**12b** for making **12C**, and **13a**/**13b** for making **13C**, respectively) (secondary structures shown in Figure S5 and S6). The structure of the final dumbbell-shaped cDNA and the stability of the stem and secondary structure-free loop regions were verified using UNAFold (Figure S4 – S6).

Supporting Information Section – 3: Ligation analysis using gel electrophoresis and observations

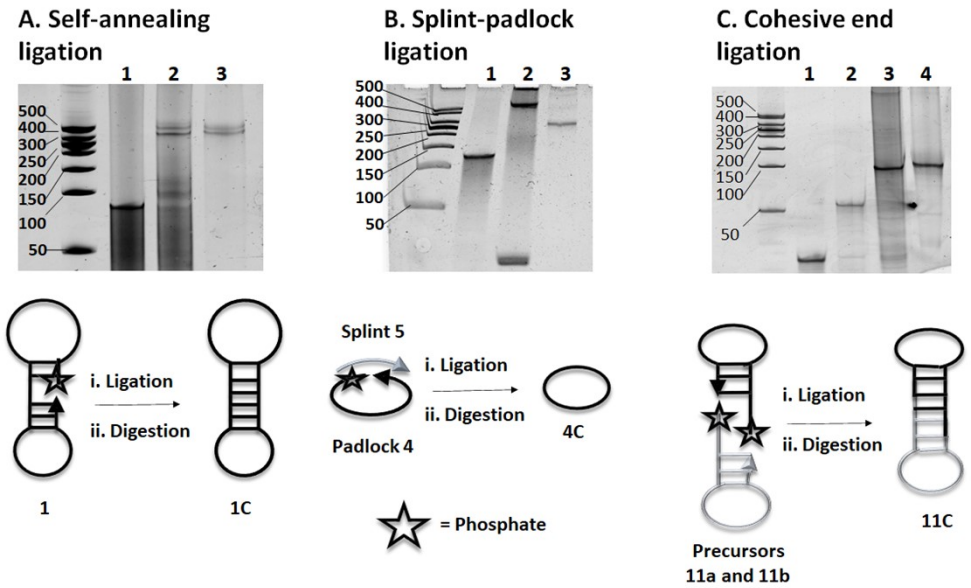

Figure S7. Analysis of cDNA synthesis in denaturing PAGE (13%). A, Analysis of self-annealing ligation synthesized cDNA **1C** using denaturing PAGE. Lane 1, unligated precursor DNA 1. Lane 2, ligation reaction for precursor DNA **1**. Lane 3, exonuclease digested (digestion condition Dig5) cDNA **1C**. B, Analysis of splint-padlock ligation synthesized cDNA **4C** using denaturing PAGE. Lane 1, unligated precursor DNA **4**. Lane 2, ligation reaction for precursor DNA **4** using splint **5** (visible in gel). Lane 3, exonuclease digested (digestion condition Dig5) cDNA **4C**. C, Analysis of cohesive end ligation synthesized cDNA **11C** using denaturing PAGE. Lane 1 and 2, unligated precursor DNA **11a** and **11b**, respectively. Lane 3, ligation reaction for precursor DNA **11a**/**11b**. Lane 4, exonuclease digested (digestion condition Dig5) cDNA **11C**. The leftmost lane in each gel contains 50 bp ladder. Each lane was loaded with 300 - 600 ng of DNA and the gel was stained with ethidium bromide before imaging

Supporting Information Section – 4: Quantification of non-specific amplification, baseline correction, normalization, and data representation

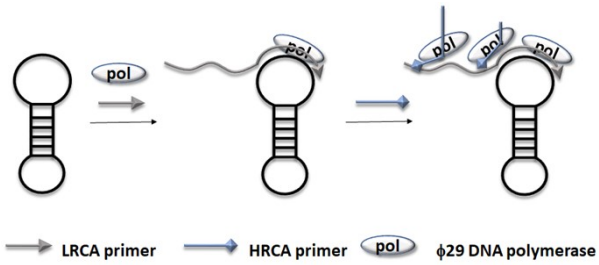

Scheme S1. Mechanism of Hyperbranched rolling circle amplification (HRCA) amplification.

4.1 Hyperbranched rolling circle amplification (HRCA). During HRCA, a primer sharing the same sequence as part of the circular DNA hybridizes to LRCA amplicon at multiple sites and initiates strand displacement amplification (Scheme S1). Using this exponentially branching amplification, HRCA significantly improves the analytical sensitivity of otherwise linear RCA by several orders of magnitude, sometimes with a detection limit as low as 100 – 1000 copies[52]. As a result, it is frequently employed in RCA assays involving both in situ ligation and pre-synthesized cDNA[52].

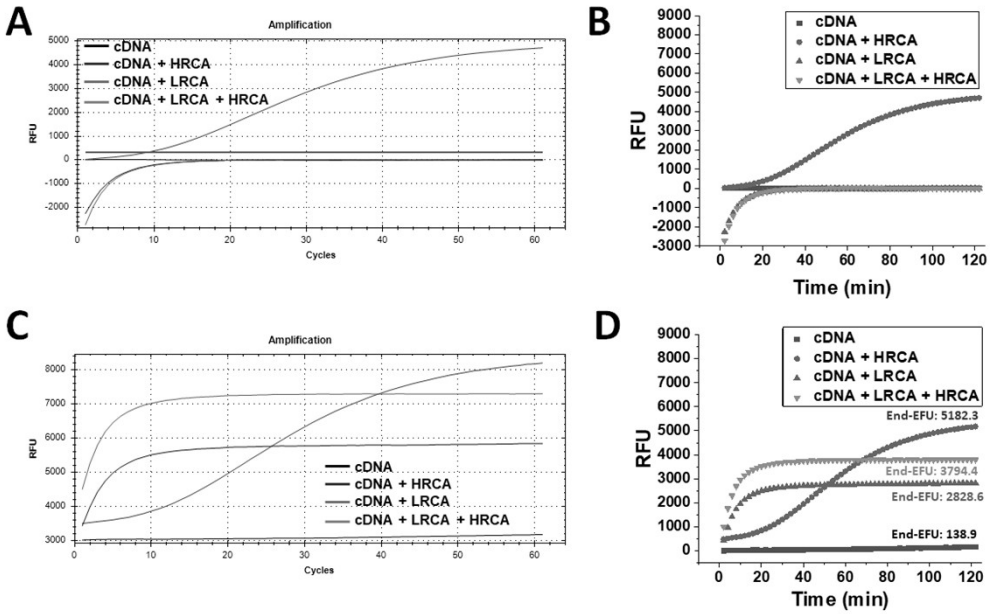

Figure S8. Method of various baseline corrections for an experiment involving representative amplification profiles of cDNA alone (no primer), cDNA with HRCA primer, cDNA with LRCA primer (referred to as LRCA in the Figure), and cDNA with both LRCA and HRCA primer. A, Mechanism of Hyperbranched rolling circle amplification (HRCA) amplification. B, Screenshots of amplification profiles with instrument software-enabled default baseline correction. C, Same experiment plotted in Origin software without any further baseline correction. D, Screenshot of the same experiment in instrument PC without any baseline correction applied by the software. E, Amplification profiles after the cycle 1 (at 2 min) fluorescence of cDNA alone sample was subtracted from the amplification fluorescence of itself and other samples. The color codes are identical for all panel. Data was obtained using **12C** as cDNA, **2** as primer, and **14** as HRCA primer following Dig6.

4.2 Baseline correction methods. Here, the measurements of non-specific amplification was carried out through both absolute (using end-RFU) and relative (using normalized non-specific amplification

or NNSA) quantifications. Rolling circle amplification (RCA), when recorded in a standard real-time PCR (rt-PCR) instrument, usually did not automatically generate either absolute or relative RFU. The proprietary software for the rt-PCR instrument, intuitively programmed to sense quantitative real-time PCR (qPCR) assays, presumably searches for an early flat baseline in an amplification curve. It then "subtracts" the baseline from the whole amplification to produce the characteristic and familiar "S"-shaped plots with initial linear baselines. However, in contrast to qPCR assays, an RCA assay may not have an early flat baseline. Instead, its fluorescence rises early in the amplification and generates a flat saturation plateau later in the assay. Due to the proprietary algorithm's propensity to sense a flat baseline, the resulting baseline subtraction led to an inverted amplification plot with negative RFU (Figure S8A and B). This misrepresentation was resolved when we removed all baseline subtraction from the amplification profiles, i.e., presented it with absolute RFU (Figure S8C).

4.3 Absolute NSA measurement. Although an informative NSA marker, an absolute end-RFU presentation would be problematic when comparing different assays due to their inherent differences. Instead, a manual subtraction of the 1st cycle RFU magnitude of "cDNA alone" control in each assay (e.g., "black" amplification profile in Figure S8C) from the rest of the amplification profiles seemed a more appropriate representation. A demonstrative example of this was plotted in Figure S8D. Accordingly, this "baseline subtraction" measure was first applied in all the assays as the "cDNA alone" control has been present in all studies. Thus, the absolute NSA would be quantified by the end-RFU of a manually-baseline-subtracted "cDNA alone" control in an LRCA assay (e.g., 182 for black square profile, Figure S8D) and that of a "cDNA with HRCA" in an HRCA assay (e.g., 5168 for red circle profile, Figure S8D).

4.4 Normalized NSA (NNSA) measurement. Besides the absolute NSA, we also wanted to quantify the NNSA for a relative valuation. This was computed by percentage ratio of the end-RFU of "cDNA alone" well with that of the primer-assisted LRCA from the same experiment (e.g., $\frac{138.9}{2828.6}\%$ = 4.9% in Figure S8D). Similarly, for hyperbranched RCA (HRCA) assays, the percentage of end-RFU of cDNA with HRCA was computed with respect to that of end-RFU for HRCA primer-assisted HRCA from the same experiment (e.g., $\frac{5182.8}{3798.7}\%$ = 136% in Figure S8D).

Supporting Information Section – 5: Data summary of non-specific amplification

Table S2. Quantification of non-specific amplification for self-annealing, splint-padlock, and cohesive end ligations

Type of ligation and circular DNA substrate	Digestion and amplification Condition	End-RFU	NNSA	In Figure
Self-annealing ligation Circular DNA **1C**	Dig1	814.5 ± 239.6	37.6 ± 14.6	Figure 1A, Figure S9A
	Dig2	446.6 ± 49	14.9 ± 2.3	Figure 1A, Figure S9B
	Dig3	268.5 ± 58.7	9.7 ± 2.6	Figure 1A, Figure S9C
	Dig4	536.3 ± 49.8	25.6 ± 4.5	Figure 1A, Figure S9D
	Dig5	-10.6 ± 4.8	-0.6 ± 0.3	Figure 2A, Figure S11A
	Dig6	76.9 ± 21.2	0.8 ± 0.2	Figure 2A, Figure S11B
	Dig7	29 ± 21.1	0.4 ± 0.3	Figure 2A, Figure S11C
	Dig8	1091.7 ± 156.1	16.5 ± 2.7	Figure 2A, Figure S11D
	Dig9	775 ± 246.8	10.2 ± 4.3	Figure 2A, Figure S11E
	Dig5 + HRCA	92.4 ± 47.1	5 ± 3.8	Figure 3A, Figure S12A
	Dig6 + HRCA	434 ± 43.9	19.2 ± 1	Figure 3A, Figure S12B
	Dig7 + HRCA	649.6 ± 96.3	24.5 ± 2.4	Figure 3A, Figure S12C
Cohesive end (14 nt cohesive end at 5'-termini) ligation Circular DNA **11C**	Dig1	928.3 ± 237.5	33 ± 9.4	Figure 1C, Figure S9I
	Dig2	1237.3 ± 214.8	40.2 ± 9.4	Figure 1C, Figure S9J
	Dig3	185.5 ± 39	6.3 ± 0.9	Figure 1C, Figure S9K
	Dig4	1346.9 ± 162.2	60.4 ± 8.1	Figure 1C, Figure S9L
	Dig5	337.3 ± 33.6	9.3 ± 4.2	Figure 2C, Figure S11K
	Dig6	122.7 ± 112.3	3.3 ± 3.3	Figure 2C, Figure S11L
	Dig7	6.8 ± 4.8	0.6 ± 0.4	Figure 2C, Figure S11M
	Dig8	2017.7 ± 326.8	21.2 ± 4.2	Figure 2C, Figure S11N
	Dig9	587 ± 159.1	8.4 ± 3.1	Figure 2C, Figure S11O
	Dig5 + HRCA	2285.3 ± 304.9	80.2 ± 15.1	Figure 3B, Figure S12D
	Dig6 + HRCA	2143.4 ± 82.2	82.1 ± 2.8	Figure 3B, Figure S12E
	Dig7 + HRCA	2243.5 ± 71.4	81.8 ± 9	Figure 3B, Figure S12F
Cohesive end (9 nt	Dig6	305.1 ± 264.9	6.1 ± 5.1	Figure 4A,

cohesive end at 5'-termini) ligation Circular DNA **12C**				Figure S13C
	Dig6 + HRCA	4752.9 ± 1002.9	106.8 ± 32.9	Figure 4A, Figure S13C
	Dig7	423.4 ± 235.2	8.5 ± 6.4	Figure 4A, Figure S13D
	Dig7 + HRCA	5168.3 ± 607.8	103.3 ± 11.8	Figure 4A, Figure S13D
Cohesive end (5 nt cohesive end at 5'-termini) ligation Circular DNA **13C**	Dig6	339.1 ± 211.8	16.3 ± 13.1	Figure 4B, Figure S13A
	Dig6 + HRCA	2159.9 ± 512.5	108 ± 53.9	Figure 4B, Figure S13A
	Dig7	303.3 ± 51.5	12.7 ± 6.1	Figure 4B, Figure S13B
	Dig7 + HRCA	2139.9 ± 73.9	72.2 ± 28.9	Figure 4B, Figure S13B
Splint-padlock (38 nt splint) ligation Circular DNA **4C**	Dig1	1210.3 ± 172.8	128.4 ± 10.6	Figure 1B, Figure S9E
	Dig2	2471.3 ± 212.3	92.3 ± 7	Figure 1B, Figure S9F
	Dig3	1218.1 ± 163.5	44.7 ± 13	Figure 1B, Figure S9G
	Dig4	1496.5 ± 148.4	203.8 ± 26.2	Figure 1B, Figure S9H
	Dig5	3116 ± 140.4	58.4 ± 12.7	Figure 2B, Figure S11F
	Dig6	3907.7 ± 616.3	77.9 ± 9.7	Figure 2B, Figure S11G
	Dig7	1896.7 ± 137.6	32.6 ± 7.4	Figure 2B, Figure S11H
	Dig8	1556.7 ± 400.5	160.8 ± 90	Figure 2B, Figure S11I
	Dig9	1904.3 ± 1149.3	143 ± 79.8	Figure 2B, Figure S11J
Splint-padlock (30 nt splint) ligation Circular DNA **4C**	Dig6	260.7 ± 97	6.9 ± 2.3	Figure 5B, Figure 15C
	Dig7	68.8 ± 13.3	4.5 ± 1.7	Figure 5C, Figure 15F
Splint-padlock (24 nt splint) ligation Circular DNA **4C**	Dig6	133.8 ± 40.2	2.9 ± 0.9	Figure 5B, Figure 15B
	Dig7	53.0 ± 28.2	3.5 ± 1.9	Figure 5C, Figure 15D
Splint-padlock (16 nt splint) (Figure 5B and C) ligation Circular DNA **4C**	Dig6	0.4 ± 0.2	0.2 ± 0.1	Figure 5B, Figure S15A
	Dig7	-9.6 ± 2.6	-0.8 ± 0.2	Figure 5C, Figure S15D
Splint-padlock (16 nt splint) (Figure 6) ligation Circular DNA **4C**	Dig6	4.9 ± 3.4	0.6 ± 0.4	Figure 6, Figure S16A
	Dig6 + HRCA	122.3 ± 35.5	5 ± 3.3	Figure 6, Figure S16A
	Dig7	21.9 ± 19.4	3.5 ± 0.8	Figure 6. Figure S16B
	Dig7 + HRCA	38.1 ± 5.8	2.1 ± 0.2	Figure 6, Figure S16B
Self-annealing ligation Circular DNA **15C**	Dig5	65.2 ± 7.3	3.8 ± 1.2	Figure 7A and Figure S20
	Dig8	132.9 ± 22.4	13.3 ± 2.4	

Splint-padlock (38 nt splint) ligation Circular DNA **16C**	Dig6	955.2 ± 82.9	94.6 ± 10.2	Figure 7B and Figure S21
	Dig8	940.0 ± 75.6	82.6 ± 8.5	
Splint-padlock (16 nt splint) ligation Circular DNA **16C**	Dig6	273.2 ± 22.4	22.1 ± 2.3	Figure 7C and Figure S22
	Dig8	60.2 ± 5.2	5.5 ± 1.2	

Supporting Information Section – 6: Representative amplification plots for Dig1 – Dig4 digestions (LRCA conditions)

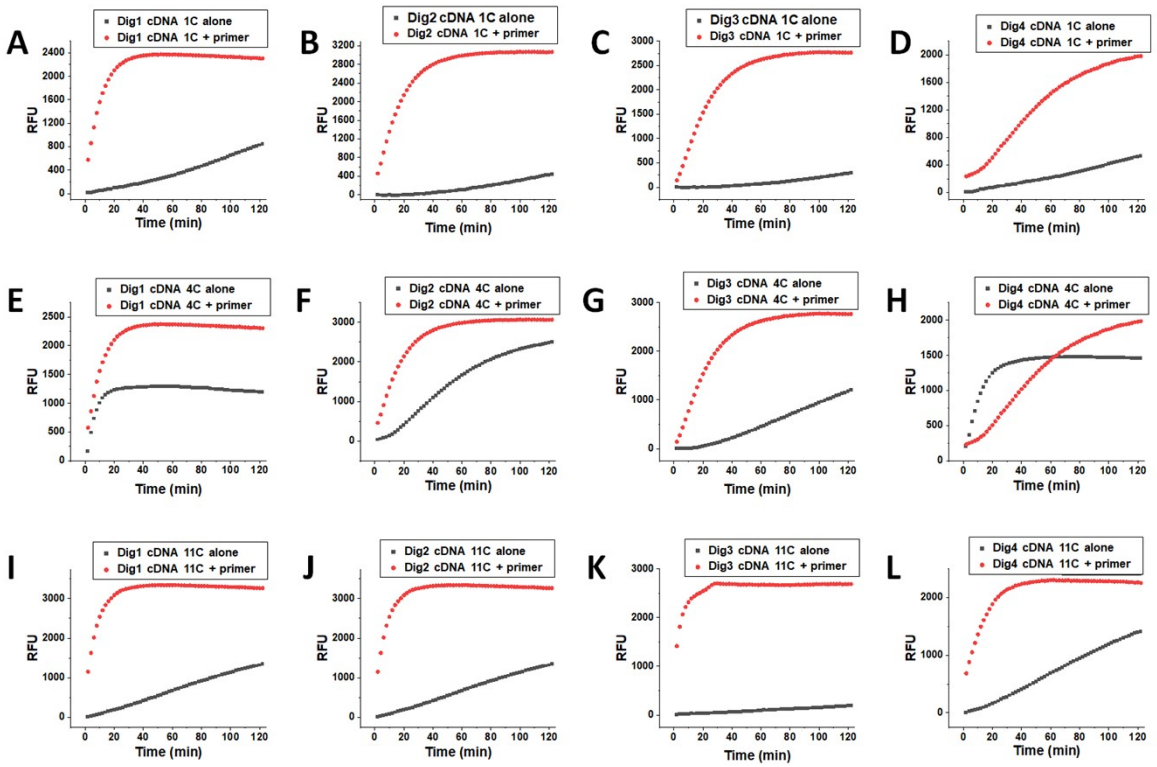

Figure S9. Representative amplification profiles for NSA measurement for exonuclease digestion conditions Dig1 – Dig4 under LRCA condition. A – D, Amplification profiles for self-annealing ligated cDNA **1C** (following Dig1 – Dig4 digestions, respectively) alone and with LRCA primer. E – H, Amplification profiles for splint-padlock ligated cDNA **4C** (following Dig1 – Dig4 digestions, respectively) alone and with LRCA primer. I – L, Amplification profiles for self-annealing ligated cDNA **11C** (following Dig1 – Dig4 digestions, respectively) alone and with LRCA primer.

Supporting Information Section – 7: Pilot studies on salt and buffer conditions used during dual Exo I and Exo III digestions

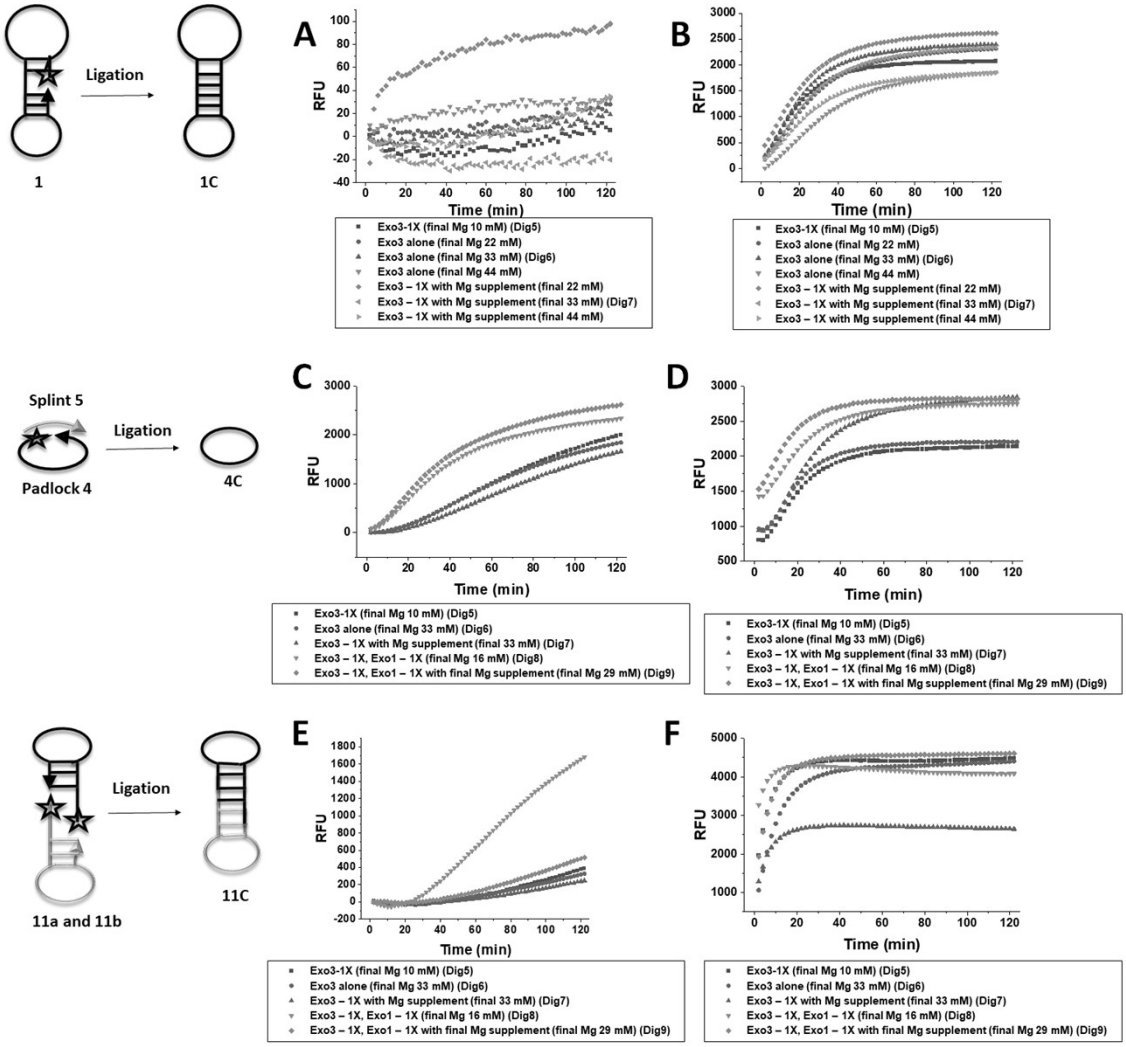

Figure S10. Pilot experiments to explore various salt and buffer compositions during dual exonuclease I and III digestion. A, Representative amplification profiles for self-annealing ligated cDNA **1C** alone for dual exonuclease digestion using Exo III buffer with its concentrations adjusted to have final total Mg^{2+} concentrations 10 – 44 mM without any supplemental Mg^{2+} addition. The same panel also has cDNA **1C** amplification profiles for dual exonuclease digestion with Exo III buffer in 1X concentration but with supplemental Mg^{2+} addition to attain final total Mg^{2+} concentrations 10 – 44 mM. B, Representative amplification profiles for cDNA **1C** with LRCA primer for same salt and buffer compositions as described in Panel A. C, Representative amplification profiles for self-annealing ligated cDNA **4C** alone for dual exonuclease digestion using Exo III buffer with concentration adjusted to have Mg^{2+} 10 or 33 mM (Dig5 and Dig6), Exo III buffer 1X with supplemental Mg^{2+} to final concentration 33 mM (Dig7), combined Exo I and III buffer in 1X concentration each (Dig8), or combined Exo I and III buffer in 1X concentration with supplemental Mg^{2+} to final concentration 29 mM (Dig9). D, Representative amplification profiles for cDNA **4C** with LRCA primer for the same salt and buffer compositions as described in Panel C. E, Representative amplification profiles for self-annealing ligated cDNA **11C** alone for the same salt and buffer compositions as described in Panel C. F, Representative amplification profiles for cDNA **11C** with LRCA primer for the same salt and buffer compositions as described in Panel C.

Supporting Information Section – 8: Representative amplification plots for Dig5 – Dig9 digestion (LRCA conditions)

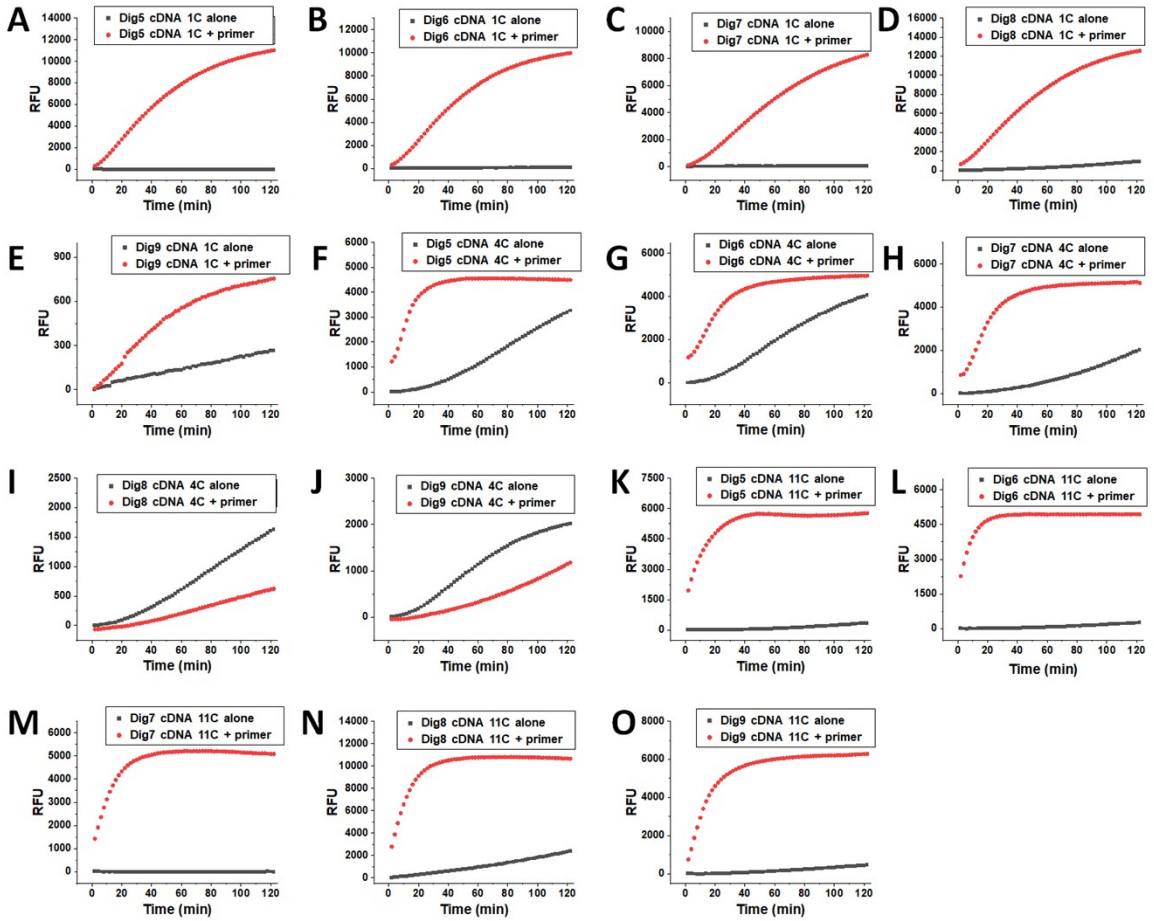

Figure S11. Representative amplification profiles for NSA measurement for exonuclease digestion conditions Dig5 – Dig9 under LRCA condition. A – E, Amplification profiles for self-annealing ligated cDNA **1C** (following Dig5 – Dig9 digestions, respectively) alone and with LRCA primer. F – J, Amplification profiles for splint-padlock ligated cDNA **4C** (following Dig5 – Dig9 digestions, respectively) alone and with LRCA primer. K – O, Amplification profiles for self-annealing ligated cDNA **11C** (following Dig5 – Dig9 digestions, respectively) alone and with LRCA primer.

Supporting Information Section – 9: Non-specific amplification under HRCA conditions for digestion Dig5 – Dig7

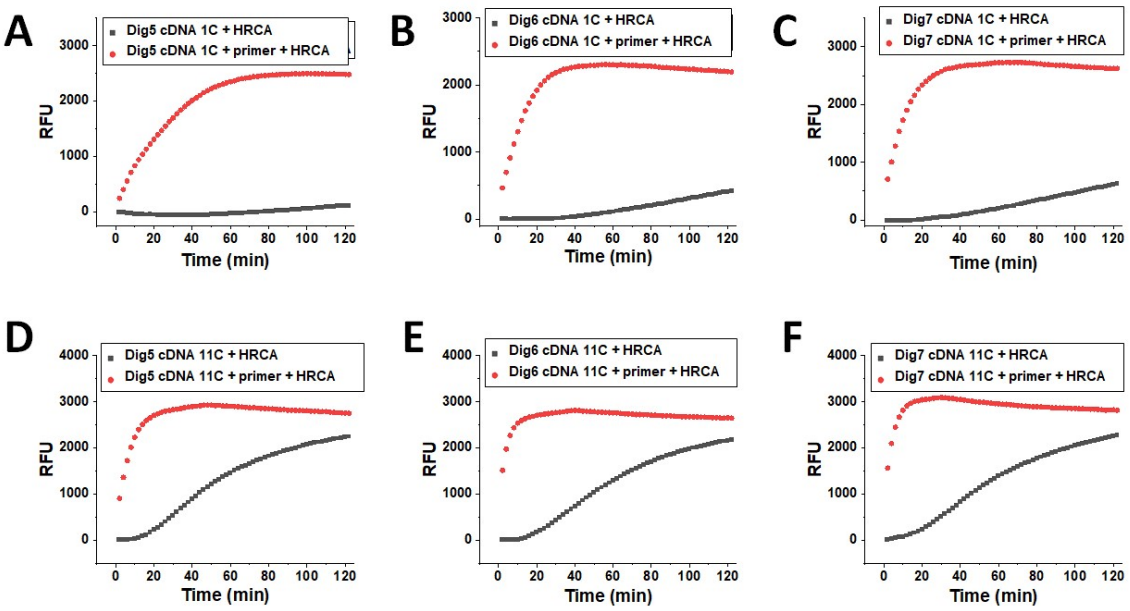

Figure S12. Representative amplification profiles for NSA measurement for exonuclease digestion conditions Dig5 – Dig7 under HRCA condition. A – C, Amplification profiles for self-annealing ligated cDNA **1C** (following Dig5 – Dig7 digestions, respectively) with HRCA alone, and with both LRCA and HRCA primer. D – F, Amplification profiles for cohesive end ligated cDNA **11C** (following Dig5 – Dig7 digestions, respectively) with HRCA alone, and with both LRCA and HRCA primer.

Supporting Information Section – 10: Non-specific amplification for 5 and 9 nt cohesive end ligated cDNAs under LRCA and HRCA conditions

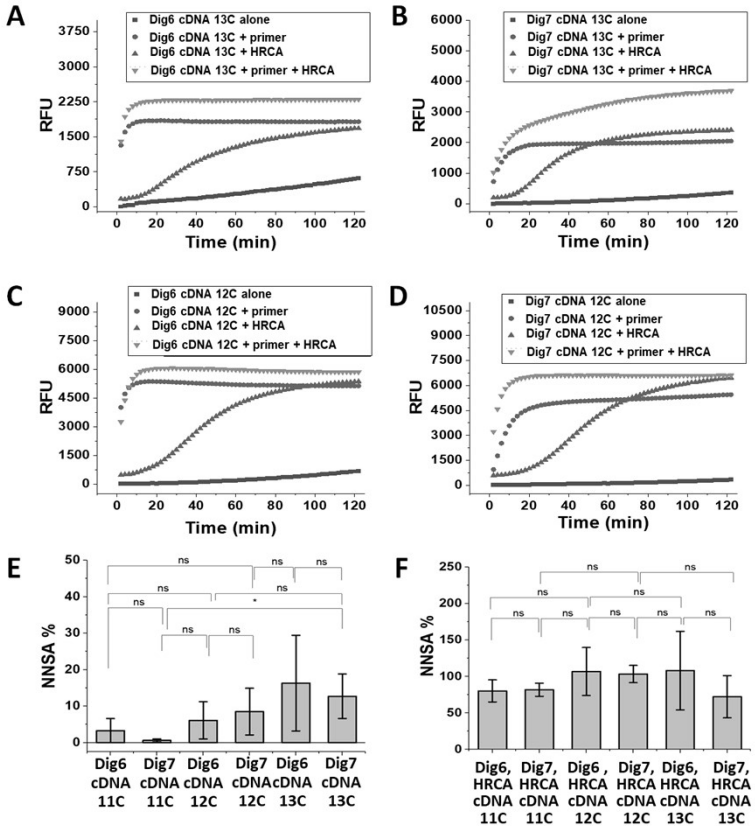

Figure S13. Representative amplification profiles for NSA measurement for exonuclease digestion conditions Dig6 – Dig7 under LRCA and HRCA conditions for shorter cohesive end enabled ligation. A and B, Amplification profiles for 5 nt 5′-termini cohesive end ligated cDNA **13C** (following Dig6 – Dig7 digestions, respectively) alone, with LRCA primer, with HRCA primer, and with both LRCA and HRCA primers. C and D, Amplification profiles for 9 nt 5′-termini cohesive end ligated cDNA **12C** (following Dig6 – Dig7 digestions, respectively) alone, with LRCA primer, with HRCA primer, and with both LRCA and HRCA primers. E and F, Comparison of NNSA % values for **11C**, **12C**, and **13C** following Dig6 and Dig7 digestions and LRCA and HRCA conditions, respectively. These panels use the same dataset as in Figure 2C, Figure 3B, and Figure 4. Error bars represent standard deviation (n = 3). *P ≤ 0.1,

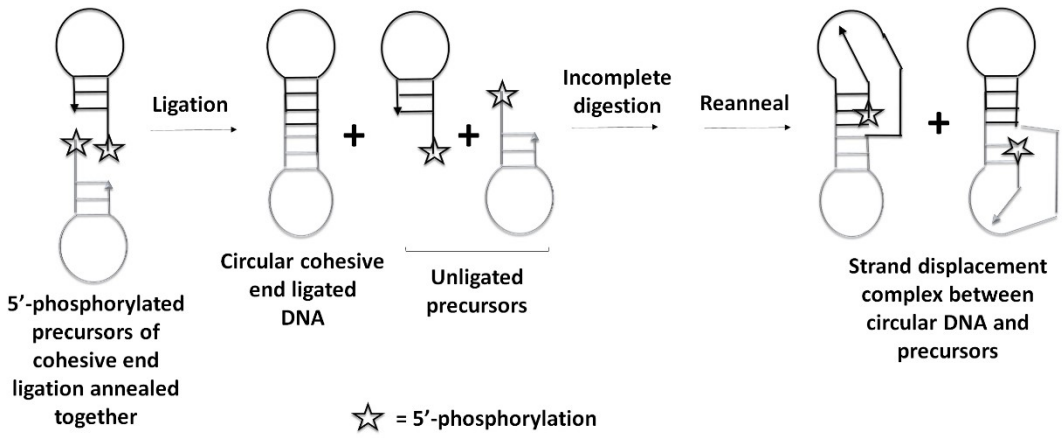

Scheme S2. Possible mechanism of strand-displacement complex formation between circular DNA and unligated precursor in cohesive end ligation.

Supporting Information Section – 11: Effect of prolonged heating and snap-cooling on non-specific amplification for splint-padlock ligation

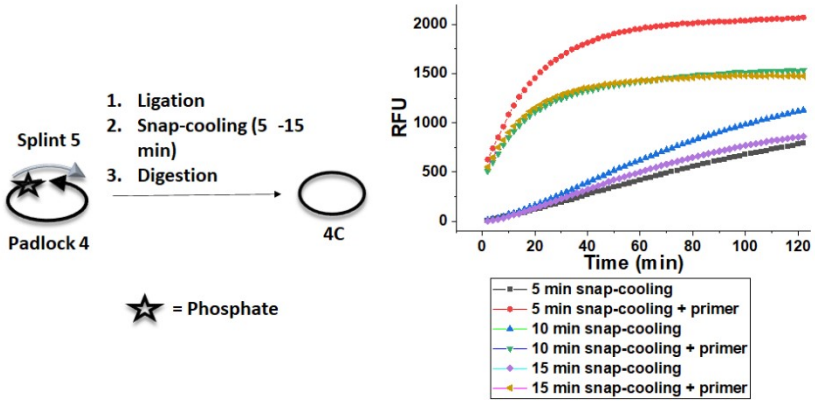

Figure S14. Representative amplification profiles for NSA measurement for 5 – 15 min snap cooling followed by dual Exo I and III dual digestion for Dig5 condition for splint-padlock ligated cDNA **4C** alone and with LRCA primer.

Supporting Information Section – 12: Effect of splint length on splint-padlock ligation (LRCA and HRCA conditions)

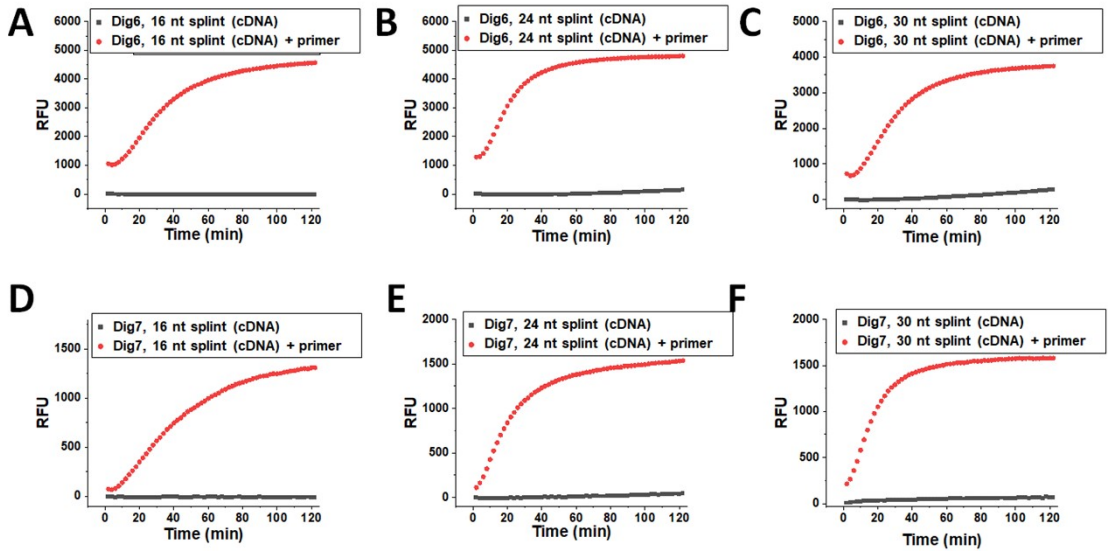

Figure S15. Representative amplification profiles for NSA measurement as a function of splint length for Dig6 – Dig7 exonuclease treatment under LRCA condition. A – C, Amplification profiles for splint-padlock ligated and Dig6 condition digested cDNA **4C** alone and with LRCA primer for splint lengths 16 – 30 nt, respectively. D – F, Amplification profiles for splint-padlock ligated and Dig7 condition digested cDNA **4C** alone and with LRCA primer for splint lengths 16 – 30 nt, respectively.

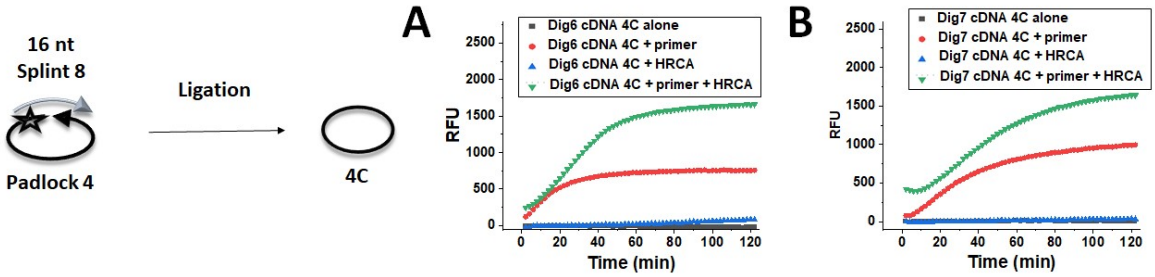

Figure S16. Representative amplification profiles for NSA measurement for 16 nt splint-padlock ligation followed by Dig6 – Dig7 exonuclease treatment under LRCA and HRCA conditions. A and B, Amplification profiles for 16 nt splint-padlock ligated cDNA **4C** (following Dig6 – Dig7 digestions, respectively) alone, with LRCA primer, with HRCA primer, and with both LRCA and HRCA primers.

Supporting Information Section – 13: Reproducibility of the methods

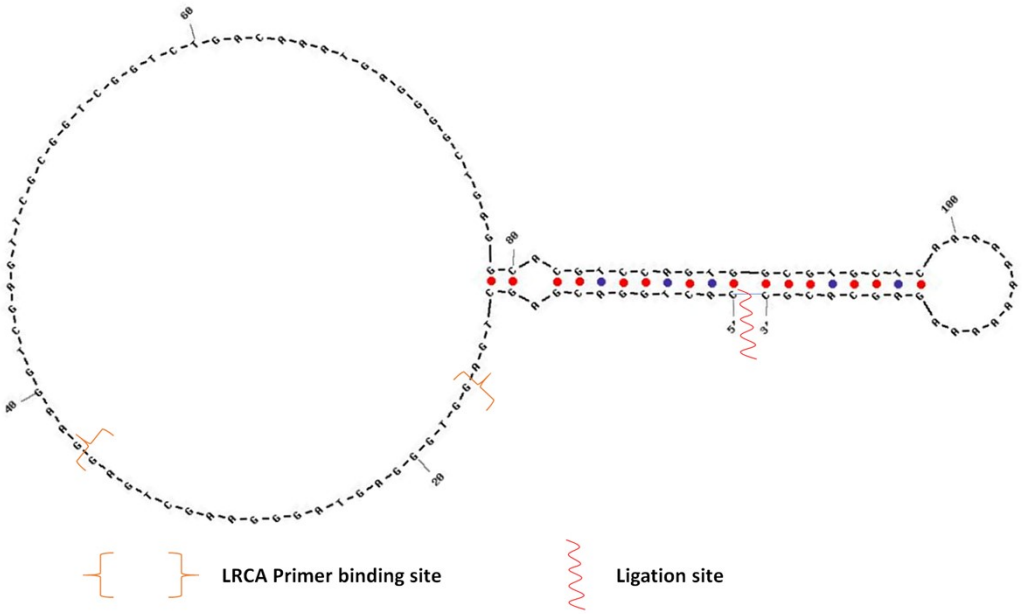

Figure S17. Secondary structure of self-annealing cDNA **15C**. The positions of the ligation site and primer binding sites are indicated. Secondary structure has been generated using UNAFold[53].

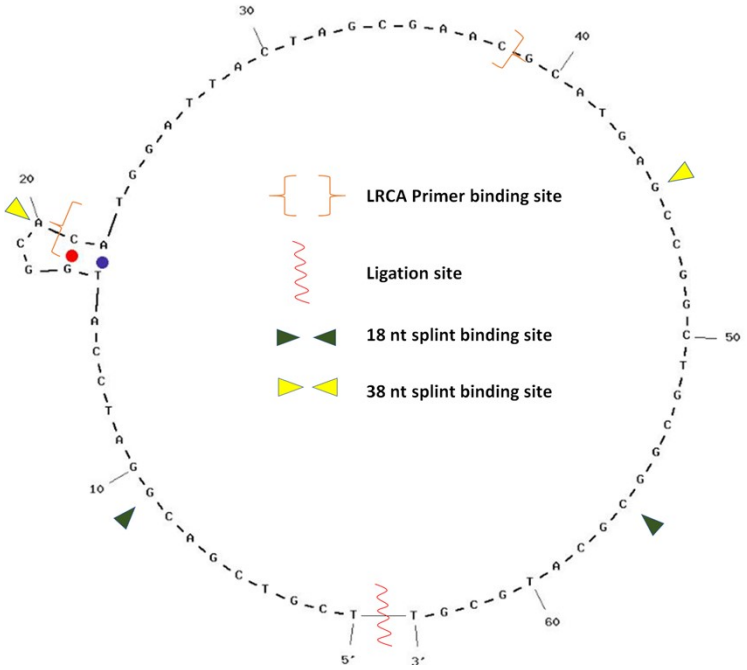

Figure S18. Secondary structure of self-annealing cDNA **16C**. The positions of the ligation site, splint binding site, and primer binding sites are indicated. Secondary structure has been generated using UNAFold[53].

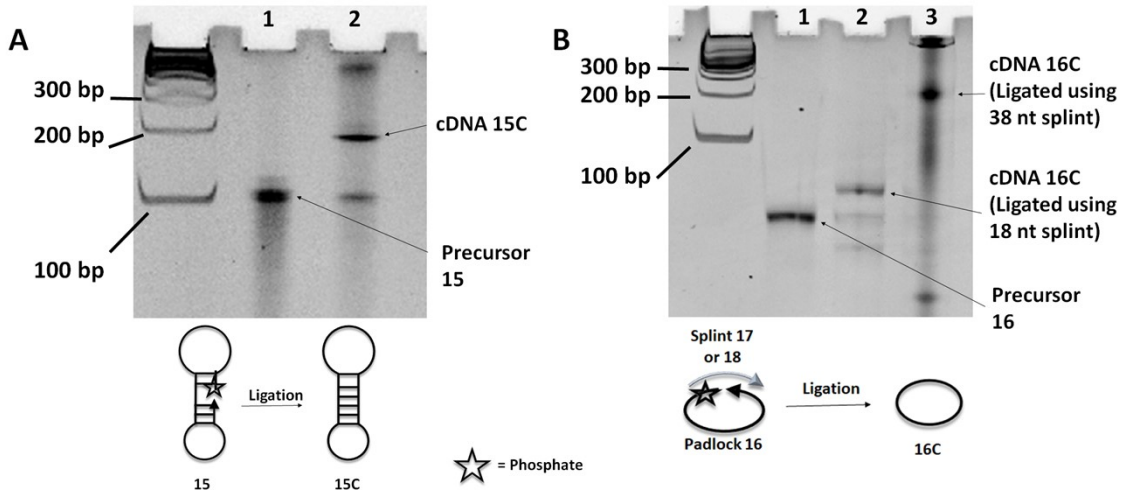

Figure S19. Gel profiles for self-annealing and splint-padlock ligation for cDNAs **15C** and **16C**, respectively. A, Analysis of self-annealing ligation synthesized cDNA **15C** using denaturing PAGE. Lane 1, unligated precursor DNA **15**. Lane 2, ligation reaction for preparing cDNA **15C**. B, Analysis of splint-padlock ligation synthesized cDNA **16C** using denaturing PAGE. Lane 1, unligated precursor DNA **16**. Lane 2, ligation reaction for preparing cDNA **16C** using 18 nt long splint **18**. Lane 3, ligation reaction for preparing cDNA **16C** using 38 nt long splint **17**.

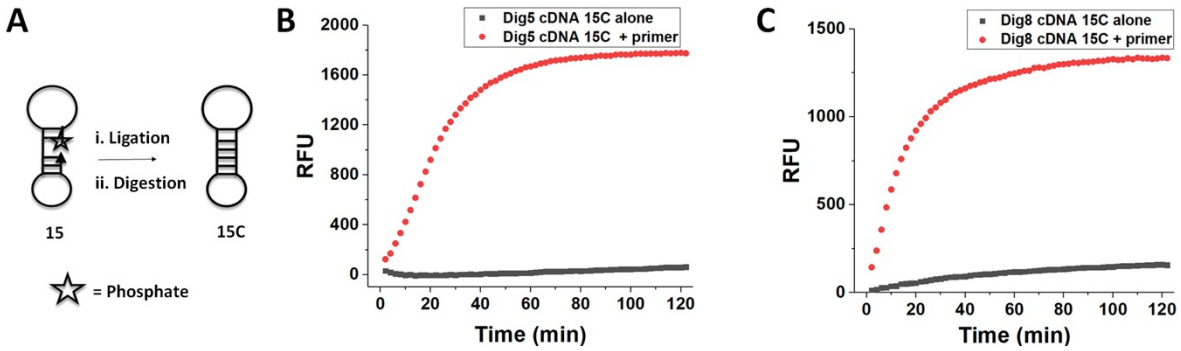

Figure S20. Representative amplification plots for self-annealing ligated cDNA **15C** (panel A) digested under conditions Dig5 (panel B) and Dig8 (Panel C). LRCA conditions and primer **19** were used.

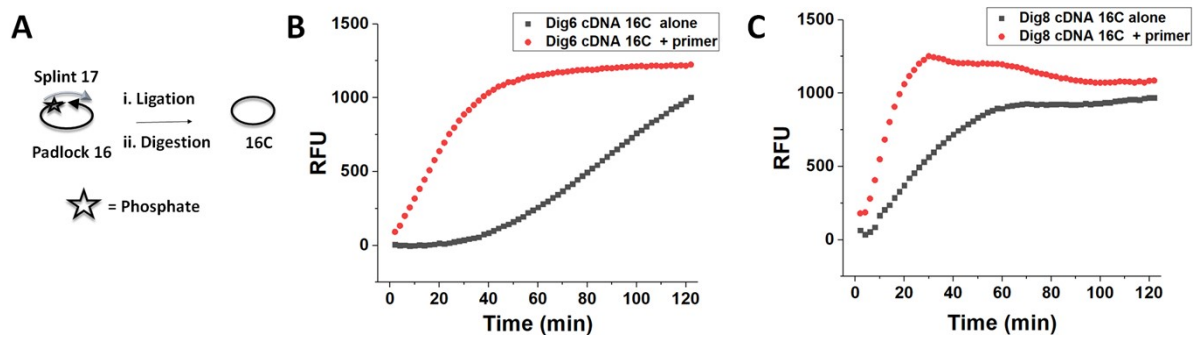

Figure S21. Representative amplification plots for splint-padlock (using long splint **17**) ligated cDNA **16C** (Panel A) digested under conditions Dig6 (panel B) and Dig8 (Panel C). LRCA conditions and primer **20** were used.

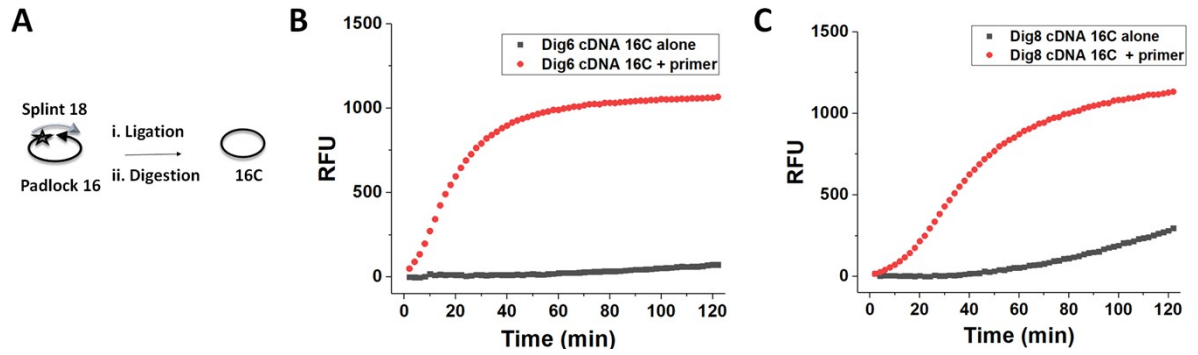

Figure S22. Representative amplification plots for splint-padlock (using short splint **18**) ligated cDNA **16C** (Panel A) digested under conditions Dig6 (panel B) and Dig8 (Panel C). LRCA conditions and primer **20** were used.

References

(1) Jiao, J.; Li, P.; Gu, Y.; Du, X.; Wang, S.; Wang, J. A Fluorescence Quenching-Recovery Sensor Based on RCA for the Specific Analysis of Fusobacterium Nucleatum. Nucleatum. *Anal. Biochem.* **2020**, *604*, 113808. https://doi.org/10.1016/j.ab.2020.113808.

(2) Liu, J.; Zhan, Z.; Liang, T.; Xie, G.; Aguilar, Z. P.; Xu, H. Dual-Signal Amplification Strategy: Universal Asymmetric Tailing-PCR Triggered Rolling Circle Amplification Assay for Fluorescent Detection of Cronobacter Spp. in Milk. *J. Dairy Sci.* **2020**, *103* (4), 3055–3065. https://doi.org/10.3168/jds.2019-17590.

(3) Qiu, X.; Guittet, O.; Mingoes, C.; El Banna, N.; Huang, M.-E.; Lepoivre, M.; Hildebrandt, N. Quantification of Cellular Deoxyribonucleoside Triphosphates by Rolling Circle Amplification and Förster Resonance Energy Transfer. *Anal. Chem.* **2019**, *91* (22), 14561–14568. https://doi.org/10.1021/acs.analchem.9b03624.

(4) Chen, L.; Zhang, Y.; Xia, Q.; Luo, F.; Guo, L.; Qiu, B.; Lin, Z. Fluorescence Biosensor for DNA Methyltransferase Activity and Related Inhibitor Detection Based on Methylation-Sensitive Cleavage Primer Triggered Hyperbranched Rolling Circle Amplification. *Anal. Chim. Acta* **2020**, *1122*, 1–8. https://doi.org/10.1016/j.aca.2020.04.061.

(5) Bialy, R. M.; Ali, M. M.; Li, Y.; Brennan, J. D. Protein-Mediated Suppression of Rolling Circle Amplification for Biosensing with an Aptamer-Containing DNA Primer. *Chem. Weinh. Bergstr. Ger.* **2020**, *26* (22), 5085–5092. https://doi.org/10.1002/chem.202000245.

(6) Smith, L. D.; Liu, Y.; Zahid, M. U.; Canady, T. D.; Wang, L.; Kohli, M.; Cunningham, B. T.; Smith, A. M. High-Fidelity Single Molecule Quantification in a Flow Cytometer Using Multiparametric Optical Analysis. *ACS Nano* **2020**, *14* (2), 2324–2335. https://doi.org/10.1021/acsnano.9b09498.
(7) Sun, X.; Wang, Y.; Zhang, L.; Liu, S.; Zhang, M.; Wang, J.; Ning, B.; Peng, Y.; He, J.; Hu, Y.; Gao, Z. CRISPR-Cas9 Triggered Two-Step Isothermal Amplification Method for E. Coli O157:H7 Detection Based on a Metal–Organic Framework Platform. *Anal. Chem.* **2020**, *92* (4), 3032–3041. https://doi.org/10.1021/acs.analchem.9b04162.
(8) Xiao, G.; Chen, B.; He, M.; Hu, B. Dual-Mode Detection of Avian Influenza Virions (H9N2) by ICP-MS and Fluorescence after Quantum Dot Labeling with Immuno-Rolling Circle Amplification. *Anal. Chim. Acta* **2020**, *1096*, 18–25. https://doi.org/10.1016/j.aca.2019.10.063.
(9) Gao, X.; Niu, S.; Ge, J.; Luan, Q.; Jie, G. 3D DNA Nanosphere-Based Photoelectrochemical Biosensor Combined with Multiple Enzyme-Free Amplification for Ultrasensitive Detection of Cancer Biomarkers. *Biosens. Bioelectron.* **2020**, *147*, 111778. https://doi.org/10.1016/j.bios.2019.111778.
(10) He, L.; Shen, Z.; Cao, Y.; Li, T.; Wu, D.; Dong, Y.; Gan, N. A Microfluidic Chip Based Ratiometric Aptasensor for Antibiotic Detection in Foods Using Stir Bar Assisted Sorptive Extraction and Rolling Circle Amplification. *Analyst* **2019**, *144* (8), 2755–2764. https://doi.org/10.1039/C9AN00106A.
(11) Zhan, Z.; Liu, J.; Yan, L.; Aguilar, Z. P.; Xu, H. Sensitive Fluorescent Detection of Listeria Monocytogenes by Combining a Universal Asymmetric Polymerase Chain Reaction with Rolling Circle Amplification. *J. Pharm. Biomed. Anal.* **2019**, *169*, 181–187. https://doi.org/10.1016/j.jpba.2019.03.016.
(12) Dong, L.; Zhang, X.; Li, Y.; E, F.; Zhang, J.; Cheng, Y. Highly Sensitive Detection of Uracil-DNA Glycosylase Activity Based on Self-Initiating Multiple Rolling Circle Amplification. *ACS Omega* **2019**, *4* (2), 3881–3886. https://doi.org/10.1021/acsomega.8b03376.
(13) Zhou, W.; Li, D.; Yuan, R.; Xiang, Y. Programmable DNA Ring/Hairpin-Constrained Structure Enables Ligation-Free Rolling Circle Amplification for Imaging MRNAs in Single Cells. *Anal. Chem.* **2019**, *91* (5), 3628–3635. https://doi.org/10.1021/acs.analchem.8b05613.
(14) Gao, T.; Li, L.; Chen, T.; Shi, L.; Yang, Y.; Li, G. DNA-Oriented Shaping of Cell Features for the Detection of Rare Disseminated Tumor Cells. *Anal. Chem.* **2019**, *91* (1), 1126–1132. https://doi.org/10.1021/acs.analchem.8b04783.
(15) Huang, F.; Chen, Y.; Wang, Y.; Xia, F. Tunable Superamphiphobic Surfaces: A Platform for Naked-Eye ATP Detection. *Anal. Bioanal. Chem.* **2019**, *411* (19), 4721–4727. https://doi.org/10.1007/s00216-018-1443-6.
(16) Gao, M.; Lian, H.; Yu, L.; Gong, M.; Ma, L.; Zhou, Y.; Yu, M.; Yan, X. Rolling Circle Amplification Integrated with Suspension Bead Array for Ultrasensitive Multiplex Immunodetection of Tumor Markers. *Anal. Chim. Acta* **2019**, *1048*, 75–84. https://doi.org/10.1016/j.aca.2018.10.001.
(17) Wang, J.; Wang, Y.; Liu, S.; Wang, H.; Zhang, X.; Song, X.; Yu, J.; Huang, J. Primer Remodeling Amplification-Activated Multisite-Catalytic Hairpin Assembly Enabling the Concurrent Formation of Y-Shaped DNA Nanotorches for the Fluorescence Assay of Ochratoxin A. *Analyst* **2019**, *144* (10), 3389–3397. https://doi.org/10.1039/C9AN00316A.
(18) Chen, Z.; Duan, X.; Wei, H.; Tang, S.; Xu, C.; Li, Y.; Guan, Y.; Zhao, G. Screening Oligonucleotide Sequences for Silver Staining and D-Galactose Visual Detection Using RCA Silver Staining in a Tube. *Acta Biochim. Biophys. Sin.* **2018**, *50* (5), 507–515. https://doi.org/10.1093/abbs/gmy034.
(19) Wu, H.; Zhou, X.; Cheng, W.; Yuan, T.; Zhao, M.; Duan, X.; Ding, S. A Simple Fluorescence Biosensing Strategy for Ultrasensitive Detection of the BCR–ABL1 Fusion Gene Based on a DNA Machine and Multiple Primer-like Rolling Circle Amplification. *Analyst* **2018**, *143* (20), 4974–4980. https://doi.org/10.1039/C8AN01094C.

(20) Gou, D.; Xie, G.; Li, Y.; Zhang, X.; Chen, H. Voltammetric Immunoassay for Mycobacterium Tuberculosis Secretory Protein MPT64 Based on a Synergistic Amplification Strategy Using Rolling Circle Amplification and a Gold Electrode Modified with Graphene Oxide, Fe3O4 and Pt Nanoparticles. *Mikrochim. Acta* **2018**, *185* (9), 436. https://doi.org/10.1007/s00604-018-2972-6.
(21) Sun, D.; Lu, J.; Luo, Z.; Zhang, L.; Liu, P.; Chen, Z. Competitive Electrochemical Platform for Ultrasensitive Cytosensing of Liver Cancer Cells by Using Nanotetrahedra Structure with Rolling Circle Amplification. *Biosens. Bioelectron.* **2018**, *120*, 8–14. https://doi.org/10.1016/j.bios.2018.08.002.
(22) Peng, X.; Liang, W.-B.; Wen, Z.-B.; Xiong, C.-Y.; Zheng, Y.-N.; Chai, Y.-Q.; Yuan, R. Ultrasensitive Fluorescent Assay Based on a Rolling-Circle-Amplification-Assisted Multisite-Strand-Displacement-Reaction Signal-Amplification Strategy. *Anal. Chem.* **2018**, *90* (12), 7474–7479. https://doi.org/10.1021/acs.analchem.8b01015.
(23) Wang, J.; Mao, S.; Li, H.-F.; Lin, J.-M. Multi-DNAzymes-Functionalized Gold Nanoparticles for Ultrasensitive Chemiluminescence Detection of Thrombin on Microchip. *Anal. Chim. Acta* **2018**, *1027*, 76–82. https://doi.org/10.1016/j.aca.2018.04.028.
(24) Kim, T.-Y.; Lim, M.-C.; Woo, M.-A.; Jun, B.-H. Radial Flow Assay Using Gold Nanoparticles and Rolling Circle Amplification to Detect Mercuric Ions. *Nanomater. Basel Switz.* **2018**, *8* (2), E81. https://doi.org/10.3390/nano8020081.
(25) Du, Y.-C.; Zhu, Y.-J.; Li, X.-Y.; Kong, D.-M. Amplified Detection of Genome-Containing Biological Targets Using Terminal Deoxynucleotidyl Transferase-Assisted Rolling Circle Amplification. *Chem. Commun.* **2018**, *54* (6), 682–685. https://doi.org/10.1039/C7CC09337C.
(26) Lv, J.; Xie, S.; Cai, W.; Zhang, J.; Tang, D.; Tang, Y. Highly Effective Target Converting Strategy for Ultrasensitive Electrochemical Assay of Hg2+. *Analyst* **2017**, *142* (24), 4708–4714. https://doi.org/10.1039/C7AN01306J.
(27) Han, S.; Lee, J. S.; Lee, J. B. Synthesis of a Multi-Functional DNA Nanosphere Barcode System for Direct Cell Detection. *Nanoscale* **2017**, *9* (37), 14094–14102. https://doi.org/10.1039/C7NR03615A.
(28) Tang, J.; Yu, Y.; Shi, H.; He, X.; Lei, Y.; Shangguan, J.; Yang, X.; Qiao, Z.; Wang, K. Polyvalent and Thermosensitive DNA Nanoensembles for Cancer Cell Detection and Manipulation. *Anal. Chem.* **2017**, *89* (12), 6637–6644. https://doi.org/10.1021/acs.analchem.7b00864.
(29) Zhang, Y.; Wang, L.; Luo, F.; Qiu, B.; Guo, L.; Weng, Z.; Lin, Z.; Chen, G. An Electrochemiluminescence Biosensor for Kras Mutations Based on Locked Nucleic Acid Functionalized DNA Walkers and Hyperbranched Rolling Circle Amplification. *Chem. Commun.* **2017**, *53* (20), 2910–2913. https://doi.org/10.1039/C7CC00009J.
(30) Xu, H.; Wu, D.; Jiang, Y.; Zhang, R.; Wu, Q.; Liu, Y.; Li, F.; Wu, Z.-S. Loopback Rolling Circle Amplification for Ultrasensitive Detection of Kras Gene. *Talanta* **2017**, *164*, 511–517. https://doi.org/10.1016/j.talanta.2016.12.017.
(31) Kühnemund, M.; Hernández-Neuta, I.; Sharif, M. I.; Cornaglia, M.; Gijs, M. A. M.; Nilsson, M. Sensitive and Inexpensive Digital DNA Analysis by Microfluidic Enrichment of Rolling Circle Amplified Single-Molecules. *Nucleic Acids Res.* **2017**, *45* (8), e59. https://doi.org/10.1093/nar/gkw1324.
(32) Stoll, H.; Steinle, H.; Stang, K.; Kunnakattu, S.; Scheideler, L.; Neumann, B.; Kurz, J.; Degenkolbe, I.; Perle, N.; Schlensak, C.; Wendel, H. P.; Avci-Adali, M. Generation of Large-Scale DNA Hydrogels with Excellent Blood and Cell Compatibility. *Macromol. Biosci.* **2017**, *17* (4), 1600252. https://doi.org/10.1002/mabi.201600252.
(33) Huang, J.; Li, X.-Y.; Du, Y.-C.; Zhang, L.-N.; Liu, K.-K.; Zhu, L.-N.; Kong, D.-M. Sensitive Fluorescent Detection of DNA Methyltransferase Using Nicking Endonuclease-Mediated Multiple Primers-like Rolling Circle Amplification. *Biosens. Bioelectron.* **2017**, *91*, 417–423. https://doi.org/10.1016/j.bios.2016.12.061.

(34) Lee, H.; Kim, D.-M.; Kim, D.-E. Label-Free Fluorometric Detection of Influenza Viral RNA by Strand Displacement Coupled with Rolling Circle Amplification. *Analyst* **2021**, *145* (24), 8002–8007. https://doi.org/10.1039/D0AN01326A.
(35) Zeng, R.; Wang, J.; Wang, Q.; Tang, D.; Lin, Y. Horseradish Peroxidase-Encapsulated DNA Nanoflowers: An Innovative Signal-Generation Tag for Colorimetric Biosensor. *Talanta* **2021**, *221*, 121600. https://doi.org/10.1016/j.talanta.2020.121600.
(36) Li, J.; Yang, F.; Jiang, B.; Zhou, W.; Xiang, Y.; Yuan, R. The Synchronization of Multiple Signal Amplifications for Label-Free and Sensitive Aptamer-Based Sensing of a Protein Biomarker. *Analyst* **2021**, *145* (24), 7858–7863. https://doi.org/10.1039/D0AN01491E.
(37) Zhou, T.; Huang, M.; Lin, J.; Huang, R.; Xing, D. High-Fidelity CRISPR/Cas13a Trans-Cleavage-Triggered Rolling Circle Amplified DNAzyme for Visual Profiling of MicroRNA. *Anal. Chem.* **2021**, *93* (4), 2038–2044. https://doi.org/10.1021/acs.analchem.0c03708.
(38) Lin, L.; Li, B.; Han, X.; Zhang, F.; Zhang, X.; Linhardt, R. J. A Rolling Circle Amplification Based Platform for Ultrasensitive Detection of Heparin. *Analyst* **2021**, *146* (2), 714–720. https://doi.org/10.1039/D0AN02061C.
(39) Pikula, M.; Ali, M. M.; Filipe, C.; Hoare, T. Single-Step Printable Hydrogel Microarray Integrating Long-Chain DNA for the Discriminative and Size-Specific Sensing of Nucleic Acids. *ACS Appl. Mater. Interfaces* **2021**, *13* (2), 2360–2370. https://doi.org/10.1021/acsami.0c21061.
(40) Zhang, B.; Li, S.; Guan, Y.; Yuan, Y. Accurate Detection of Target MicroRNA in Mixed Species of High Sequence Homology Using Target-Protection Rolling Circle Amplification. *ACS Omega* **2021**, *6* (2), 1516–1522. https://doi.org/10.1021/acsomega.0c05279.
(41) Baba, S. A.; Jain, S.; Navani, N. K. A Reliable, Quick and Universally Applicable Method for Monitoring Aptamer SELEX Progress. *Gene* **2021**, *774*, 145416. https://doi.org/10.1016/j.gene.2021.145416.
(42) Yan, Y.; Qiao, Z.; Hai, X.; Song, W.; Bi, S. Versatile Electrochemical Biosensor Based on Bi-Enzyme Cascade Biocatalysis Spatially Regulated by DNA Architecture. *Biosens. Bioelectron.* **2021**, *174*, 112827. https://doi.org/10.1016/j.bios.2020.112827.
(43) Cai, R.; Zhang, S.; Chen, L.; Li, M.; Zhang, Y.; Zhou, N. Self-Assembled DNA Nanoflowers Triggered by a DNA Walker for Highly Sensitive Electrochemical Detection of Staphylococcus Aureus. *ACS Appl. Mater. Interfaces* **2021**, *13* (4), 4905–4914. https://doi.org/10.1021/acsami.0c22062.
(44) Ford, A.; Miller, L.; Trant, J.; Nawarathne, I. N. Generating Single-Stranded DNA Circles with Minimal Resources. *MethodsX* **2021**, *8*, 101300. https://doi.org/10.1016/j.mex.2021.101300.
(45) You, M.; Peng, P.; Xue, Z.; Tong, H.; He, W.; Mao, P.; Liu, Q.; Yao, C.; Xu, F. A Fast and Ultrasensitive ELISA Based on Rolling Circle Amplification. *Analyst* **2021**, *146* (9), 2871–2877. https://doi.org/10.1039/D1AN00355K.
(46) Wang, L.; Zeng, H.; Yang, X.; Chen, C.; Ou, S. Integrated Nicking Enzyme-Powered Numerous-Legged DNA Walker Prepared by Rolling Circle Amplification for Fluorescence Detection of MicroRNA. *Microchim. Acta* **2021**, *188* (6), 214. https://doi.org/10.1007/s00604-021-04875-1.
(47) Luo, N.; Xia, Q.; Zhang, L.; Zhang, Y.; Huang, L.; Zhang, Y.; Zhao, J.; Ding, S.; Cheng, W. One-Step Discrimination of BCR/ABLp210 Transcript Isoforms Directly from RNA Extraction with Fusion-Triggered Rolling Circle Amplification. *Anal. Chim. Acta* **2019**, *1067*, 129–136. https://doi.org/10.1016/j.aca.2019.03.055.
(48) Wei, H.; Tang, S.; Hu, T.; Zhao, G.; Guan, Y. Production of Dumbbell Probe through Hairpin Cleavage-Ligation and Increasing RCA Sensitivity and Specificity by Circle to Circle Amplification. *Sci. Rep.* **2016**, *6*, 29229. https://doi.org/10.1038/srep29229.
(49) Di Giusto, D. A.; Wlassoff, W. A.; Gooding, J. J.; Messerle, B. A.; King, G. C. Proximity Extension of Circular DNA Aptamers with Real-Time Protein Detection. *Nucleic Acids Res.* **2005**, *33* (6), e64. https://doi.org/10.1093/nar/gni063.
(50) Zuker, M. Mfold Web Server for Nucleic Acid Folding and Hybridization Prediction. *Nucleic Acids Res.* **2003**, *31* (13), 3406–3415. https://doi.org/10.1093/nar/gkg595.

(51) Zadeh, J. N.; Steenberg, C. D.; Bois, J. S.; Wolfe, B. R.; Pierce, M. B.; Khan, A. R.; Dirks, R. M.; Pierce, N. A. NUPACK: Analysis and Design of Nucleic Acid Systems. *J. Comput. Chem.* **2011**, *32* (1), 170–173. https://doi.org/10.1002/jcc.21596.
(52) Lizardi, P. M.; Huang, X.; Zhu, Z.; Bray-Ward, P.; Thomas, D. C.; Ward, D. C. Mutation Detection and Single-Molecule Counting Using Isothermal Rolling-Circle Amplification. *Nat. Genet.* **1998**, *19* (3), 225–232. https://doi.org/10.1038/898.
(53) Markham, N. R.; Zuker, M. DINAMelt Web Server for Nucleic Acid Melting Prediction. *Nucleic Acids Res.* **2005**, *33* (Web Server issue), W577-581. https://doi.org/10.1093/nar/gki591.